

## Coarsening dynamics of dewetting films

K. B. Glasner\*

*Department of Mathematics, The University of Arizona, 617 North Santa Rita, Tucson, Arizona, 85721*

T. P. Witelski†

*Department of Mathematics and Center for Nonlinear and Complex Systems, Duke University, Durham, North Carolina 27708-0320*

(Received 6 May 2002; published 10 January 2003)

Lubrication theory for unstable thin liquid films on solid substrates is used to model the coarsening dynamics in the long-time behavior of dewetting films. The dominant physical effects that drive the fluid dynamics in dewetting films are surface tension and intermolecular interactions with the solid substrate. Instabilities in these films lead to rupture and other morphological changes that promote nonuniformity in the films. Following the initial instabilities, the films break up into near-equilibrium droplets connected by an ultrathin film. For longer times, the fluid will undergo a coarsening process in which droplets both move and exchange mass on slow time scales. The dynamics of this coarsening process will be obtained through the asymptotic reduction of the long-wave PDE governing the thin film to a set of ODEs for the evolution of the droplets. From this, a scaling law that governs the coarsening rate is derived.

DOI: 10.1103/PhysRevE.67.016302

PACS number(s): 47.20.Ma, 68.15.+e, 68.55.-a

### I. INTRODUCTION

The study of instabilities of thin fluid films on solid substrates is of great importance in understanding coating flows used in many industrial processes. These instabilities lead to rupture, the formation of dry spots, and further morphological changes that promote nonuniformity in the film; this dynamical behavior in unstable thin films is generally called “dewetting.” Experimental studies have shown this behavior in polymer films [1–6], liquid crystal films [7–9], liquid metals [7,10], and evaporating films [11,12]. During these dewetting processes, droplets are formed which are connected by ultrathin films. In analogy to spinodal decomposition described by the Cahn-Hilliard equation [13], this evolution is sometimes called spinodal dewetting [12,14,15].

Recent experimental and theoretical work on dewetting films has focused on the details of instability and pattern formation in the early stages of the dewetting process. This process, which starts with near-rupture of the fluid layer, eventually produces an array of holes or “dry spots” in the film which become wider over time [16]. In theoretical work, it has been suggested that the propagation of the initial instability of a flat film may be controlled by either linear or nonlinear mechanisms [17–22]. Eventually the rims of the growing holes merge, giving rise to polygonal-shaped networks of fluid ridges [2,23]. These ridges are themselves unstable, and eventually break into isolated droplets, whose structure has been studied [15,24].

The dominant physical effects that drive the fluid dynamics in this problem are surface tension and intermolecular interactions with the solid substrate [25]; the dynamics of this problem for long times will be analyzed using a simplified mathematical model. In this paper, we explore the long-time asymptotics of a one-dimensional lubrication model for

this physical system, in which isolated droplets formed in the initial stages of dewetting slowly move and exchange mass to “coarsen” and yield fewer, larger droplets.

In the limit of low Reynolds number, the Navier-Stokes equations for the flow of a very thin, slowly varying film of viscous liquid can be reduced to an evolution equation for the film thickness,  $h = h(x, y, t)$ , using lubrication theory [26,27]. This is a long-wave theory that holds for smooth, slowly varying fluid layers on solid surfaces, in the limits of small thickness and small gradients of  $h$ . In nondimensional form, the model is a nonlinear fourth-order parabolic diffusion equation [27]

$$\frac{\partial h}{\partial t} = \nabla \cdot (h^3 \nabla p), \quad (1.1)$$

where the hydrodynamic pressure  $p$  in the thin film is given by

$$p = \Pi(h) - \nabla^2 h. \quad (1.2)$$

The Laplacian term in Eq. (1.2) gives the linearized contribution of surface tension to the total pressure due to a slowly varying curved fluid interface. The combined effects of all intermolecular forces, such as van der Waals interactions and Born repulsion, for a homogeneous film of thickness  $h$  on a solid substrate is given by the disjoining pressure, the derivative of the potential  $U(h)$ ,

$$\Pi(h) \equiv \frac{dU}{dh}. \quad (1.3)$$

The form of the intermolecular potential for interactions between the liquid film and the solid substrate can be derived using density functional theory [28,29]. Many studies in fluid dynamics have used lubrication models incorporating disjoining pressures to describe the dynamics of wetting and contact line motion [30] and other problems [12,27,31–36]. More recently, similar models have been rederived using a

\*Electronic address: kglasner@math.arizona.edu

†Electronic address: witelski@math.duke.edu

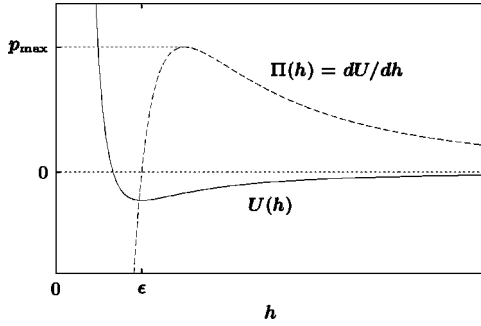


FIG. 1. Sketch of the intermolecular potential  $U(h)$  and the disjoining pressure  $\Pi(h) = dU/dh$ .

variational, diffuse-interface approach [37,38]. We will make use of a scaled form of an intermolecular potential that can be derived from the fundamental physics of intermolecular forces [28,29]. However, we will show that our analysis applies to broader classes of potentials, with applications to coarsening problems in other physical systems.

Our analysis will describe the dynamics of coarsening for a class of problems described by any potential function that satisfies a few general assumptions. We only need to assume the following in the structure of the potential  $U(h)$ :

$$U(h) \text{ has a unique minimum at } h = \epsilon, \quad (1.4)$$

$$\Pi(h) \text{ has a unique maximum, } p_{\max}, \text{ at } h_{\text{peak}} > \epsilon, \quad (1.5)$$

$$\Pi(h) = o(h^{-1}) \text{ and } U(h) \rightarrow 0 \text{ as } h \rightarrow \infty, \quad (1.6)$$

$$\lim_{h \rightarrow 0} U(h) = \infty. \quad (1.7)$$

Figure 1 shows a typical plot of the potential  $U(h)$  and the corresponding disjoining pressure  $\Pi(h)$ . Property (1.4) defines the film thickness  $h = \epsilon$  corresponding to the globally stable homogeneous film. The value of  $\epsilon$  establishes the scale of the ultrathin film (UTF) which will connect metastable liquid droplets formed after the destabilization of the initial fluid layer. Property (1.5) states that there is a film thickness for which conjoining and disjoining pressures balance; this is necessary for there to exist stable localized droplet solutions [24]. Property (1.6) requires that the disjoining pressure is negligible for thick films,  $h \gg \epsilon$ . Finally, Eq. (1.7) states that the short-range repulsive intermolecular forces are assumed to be dominant at very short scales. Early studies of van der Waals driven instabilities of thin films by Williams and Davis [33,34] and de Gennes [30] did not include repulsive interactions, and in this case classical solutions of Eq. (1.1) can cease to exist in finite time due to singularities which occur if the film ruptures,  $h \rightarrow 0$  [39,40]. In contrast, with the short-range repulsive forces corresponding to Eq. (1.7) the problem is globally well posed [24] and solutions exist for all times.

One focus of this paper is to consider the limit of small  $\epsilon$  while simultaneously keeping the interaction energies finite. To this end, we will suppose that the potential can be written in the form

$$U(h) = \mathcal{U}(h/\epsilon), \quad (1.8)$$

where the function  $\mathcal{U}$  is independent of  $\epsilon$ . This scaling is also chosen to ensure that the *gradients* of equilibrium and near-equilibrium solutions remain bounded, as is shown in the following section. This provides a *posteriori* justification for using the lubrication approximation. In contrast, in the study [24], the energy of the ultrathin film scaled like some negative power of  $\epsilon$ , leading to equilibrium droplet solutions which approached  $\delta$  functions as  $\epsilon \rightarrow 0$ .

Property (1.4) implies that the function  $\mathcal{U}(H)$  with  $H = h/\epsilon$  has a unique minimum at  $H = 1$ , and property (1.6) states that the disjoining pressure satisfies  $\Pi(h) = \epsilon^{-1} \mathcal{U}'(h/\epsilon) = o(\epsilon/h)$  as  $h \rightarrow \infty$ . A potential which satisfies all of the above assumptions is given by

$$\mathcal{U}(H) = \frac{H^{-(m-1)}}{m-1} - \frac{H^{-(n-1)}}{n-1}, \quad (1.9)$$

with  $1 < n < m$ , which yields the effective conjoining and disjoining pressure

$$\Pi(h) = \epsilon^{-1} \left( \frac{\epsilon}{h} \right)^n \left[ 1 - \left( \frac{\epsilon}{h} \right)^{m-n} \right]. \quad (1.10)$$

For this model, the maximum pressure  $p_{\max} = O(\epsilon^{-1})$  is achieved at  $h_{\text{peak}} = (m/n)^{1/(m-n)} \epsilon$ , and the absolute minimum pressure for  $h \geq \epsilon$  is  $\Pi(\epsilon) = 0$ . This particular potential was considered in Ref. [24], and with the exponents  $(n, m) = (3, 9)$  it corresponds to the standard 6–12 Lennard-Jones potential [14,15,25,27]. For numerical simulations in this paper, we will use the model (1.10) with  $(n, m) = (3, 4)$ , as has appeared in other studies of dewetting films [12,24,27,31].

We will restrict attention to the one-dimensional problem

$$\frac{\partial h}{\partial t} = \frac{\partial}{\partial x} \left( h^3 \frac{\partial}{\partial x} \left[ \Pi(h) - \frac{\partial^2 h}{\partial x^2} \right] \right). \quad (1.11)$$

In working with this problem, it is convenient to study the solution in terms of the pressure

$$p \equiv \Pi(h) - h_{xx} = \epsilon^{-1} \mathcal{U}'(h/\epsilon) - h_{xx}, \quad (1.12)$$

and the flux

$$J \equiv -h^3 p_x. \quad (1.13)$$

Numerical simulations of thin films with intermolecular forces show complex pattern formation during which films evolve to a metastable state composed of a collection of droplets connected by the UTF layer of thickness approximately  $\epsilon$ , see Fig. 4. A comparison with physical experiments shows striking similarities to the characteristic features of dewetting including the formation of capillarity ridges at the edges of growing holes (cf. [41]) as well as the development of polygonal ridge structures [2].

There is considerable similarity between Eq. (1.11) and the Cahn-Hilliard equation [13] whose late-time behavior represents the coarsening of regions of phase separation in binary alloys. The important differences are as follows.

(i) The potential  $U(h)$  has only a single minimum, whereas Cahn-Hilliard dynamics usually considers a potential with two minima.

(ii) The mobility coefficient in Eq. (1.11),  $h^3$  is nearly degenerate for  $h \rightarrow \epsilon$ , which leads to different relaxation time scales for the droplets [where  $h = O(1)$ ] and for the UTF regions [where  $h = O(\epsilon)$ ]. The original statement of the Cahn-Hilliard equation [13] included nonconstant mobilities, and has been the subject of recent studies [42].

The limiting behavior of Cahn-Hilliard-type equations are frequently expressed as free boundary problems, as was formally derived by Pego [43]. In the context of a distinguished asymptotic limit, our equation will also yield a similar type of finite-dimensional ODE approximation.

A further asymptotic regime of Cahn-Hilliard dynamics is described by the theories of Lifshitz and Slyozov [44] and Wagner [45], who characterize the statistical evolution of the phase separated regions (this is known popularly as ‘‘LSW theory’’). Mitlin [46,47] has proposed and studied a LSW-type model of coarsening behavior in fluid dewetting. We also study the statistics of dewetting using our finite-dimensional approximation.

In the following section, we begin with an analysis of the form of the structure of the equilibrium droplet solutions. In Sec. III, energetic arguments are used to describe the expected long-time dynamics. In Sec. IV, evolution equations are derived for a single near-equilibrium droplet in response to externally imposed fluxes. These evolution equations are then extended to describe the dynamics of arrays of interacting droplets in Sec. V. And finally, in Sec. VI a scaling law is derived to describe coarsening in very large sets of droplets.

## II. STEADY-STATE SOLUTIONS

Stable steady solutions of Eq. (1.11) which represent isolated fluid droplets were analyzed previously [24], and we briefly review them here. Nontrivial steady-state solutions of Eq. (1.11) have uniform, constant pressure  $p = \bar{p} \geq 0$ , and consequently  $h = \bar{h}(x; \bar{p})$  satisfies the second-order ordinary differential equation

$$\frac{d^2 \bar{h}}{dx^2} = \Pi(\bar{h}) - \bar{p}. \quad (2.1)$$

Given the structure of  $\Pi(h)$  for any value of  $\bar{p}$  in the range  $0 < \bar{p} < p_{\max}$ , a phase plane analysis shows that an isolated droplet on an unbounded domain is given by the homoclinic solution of Eq. (2.1), see Fig. 2. The maximum pressure  $p_{\max} = \Pi(h_{\text{peak}}) = O(\epsilon^{-1})$  is large, and there is a continuous family of droplet solutions parametrized by the pressure  $\bar{p}$ . For any fixed, finite pressure in this range,  $\bar{p} = O(1)$ , the minimum thickness of film in the droplet solution is the  $O(\epsilon)$  fixed point of Eq. (2.1), the root of the equation

$$\Pi(h_{\min}) = \bar{p}, \quad (2.2)$$

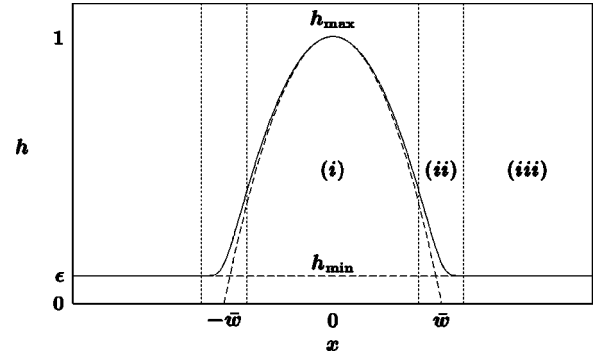


FIG. 2. A stable steady-state droplet solution  $\bar{h}(x; \bar{p})$  showing the three regions in the asymptotic structure of the solution for  $\epsilon \rightarrow 0$ : (i) the droplet core, (ii) the contact line, and (iii) the outer ultrathin film. The dashed curve shows the leading order asymptotic solution for the droplet core, the parabola (2.7), with width  $2\bar{w}$ .

this value determines the thickness of the ultrathin film far away from the droplet. Once  $h_{\min}(\bar{p})$  is determined, we can write the first integral of Eq. (2.1) as

$$\frac{1}{2} \left( \frac{d\bar{h}}{dx} \right)^2 = R(\bar{h}), \quad (2.3)$$

where

$$R(\bar{h}) \equiv U(\bar{h}) - U(h_{\min}) - \bar{p}(\bar{h} - h_{\min}). \quad (2.4)$$

At the maximum of the droplet  $\bar{h}_x = 0$  at  $x = 0$ , and hence  $h_{\max}$  is determined by the condition

$$R(h_{\max}) = 0. \quad (2.5)$$

The values of  $h_{\min}$ ,  $h_{\max}$  may be obtained graphically by constructing the tangent-secant line with slope  $\bar{p}$  for the potential  $U(h)$ , see Fig. 3. The homoclinic solution can then be obtained from Eq. (2.3) via quadrature.

To get more insight into the droplet solutions, we consider their asymptotic properties for the limit  $\epsilon \rightarrow 0$ . In the limit  $\epsilon \rightarrow 0$ , the structure of the solution breaks down into three regimes [24] (see Fig. 2): (i) *the droplet core* containing the bulk of the fluid mass, (ii) *the contact line* where asymptotic matching between the core and the outer film takes place, and (iii) *the outer region*, the uniform ultrathin film that extends indefinitely away from the base of the droplet.

In region (iii), away from the droplet core, the ultrathin film differs from the minimum thickness by exponentially small terms,  $\bar{h}(x) \sim h_{\min}(\bar{p})$ . To leading order,  $h_{\min} \sim \epsilon$  and solving Eq. (2.2) to next order as  $\epsilon \rightarrow 0$  yields the dependence on the pressure,

$$h_{\min}(\bar{p}) \sim \epsilon + \epsilon^2 \frac{\bar{p}}{\mathcal{U}''(1)}. \quad (2.6)$$

Moreover, from Eq. (2.5) we also obtain that the droplet core satisfies  $h_{\max}(\bar{p}) \sim -\mathcal{U}(1)/\bar{p}$ . In the core region, the film thickness satisfies  $\epsilon \ll \bar{h} \leq h_{\max}$ , consequently the disjoining

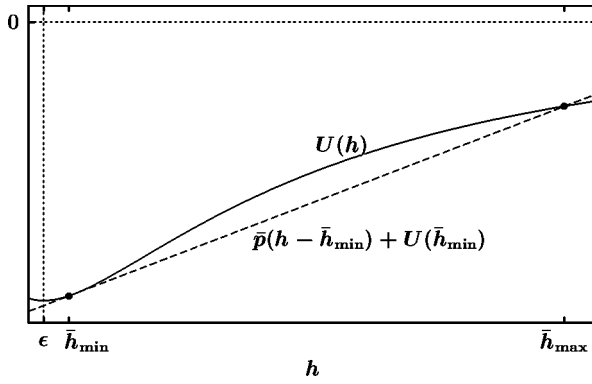


FIG. 3. Construction of  $h_{\min}$  and  $h_{\max}$  from the potential  $U(h)$  for a droplet solution with a given value of the pressure  $\bar{p}$ .

pressure is negligible,  $\Pi(\bar{h}) = o(1)$ . Therefore, in the core, the leading order solution of Eq. (2.1) is a parabolic profile (see Fig. 2),

$$\bar{h}(x) \sim \frac{1}{2\bar{p}}(\bar{w}^2 - x^2), \quad \text{for } |x| \ll |\bar{w}|, \quad (2.7)$$

where the parameter  $\bar{w}$  gives an effective measure of the width of the droplet. From Eq. (2.7), the maximum is given by  $h_{\max} \sim \frac{1}{2}\bar{p}\bar{w}^2$ . From this and the earlier estimate of  $h_{\max}(\bar{p})$ , we obtain the core width as

$$\bar{w}(\bar{p}) = \frac{A}{\bar{p}}, \quad A \sim \sqrt{2|\mathcal{U}(1)|}. \quad (2.8)$$

Further interpretation of the constant  $A$  is provided by examining the contact line, region (ii). In this region, where the droplet core must asymptotically match to the ultrathin film, we rescale the film thickness as  $\bar{h}(x) = \epsilon\bar{H}(z)$ , in a small neighborhood of the edge of the core,  $x = -\bar{w} + \epsilon z$ . Using these scalings, to leading order as  $\epsilon \rightarrow 0$ , Eq. (2.1) reduces to

$$\frac{d^2\bar{H}}{dz^2} = \mathcal{U}'(\bar{H}), \quad (2.9)$$

and the local structure of the droplet contact line is given by the transition layer solution that satisfies  $\bar{H}(z \rightarrow -\infty) \rightarrow 1$  and matches to the core region,  $\bar{H}(z \rightarrow \infty) = O(\epsilon^{-1}) \rightarrow \infty$ . Analogous to Eq. (2.3), the first integral of the leading order equation (2.9) is

$$\frac{1}{2} \left( \frac{d\bar{H}}{dz} \right)^2 = \mathcal{U}(\bar{H}) - \mathcal{U}(1). \quad (2.10)$$

Asymptotic matching of the slope of the solution for  $z \rightarrow \infty$  then yields a measure of the macroscopic contact angle,

$$\left. \frac{d\bar{h}}{dx} \right|_{-w} = \lim_{z \rightarrow \infty} \frac{d\bar{H}}{dz} = \sqrt{2|\mathcal{U}(\infty) - \mathcal{U}(1)|} = A. \quad (2.11)$$

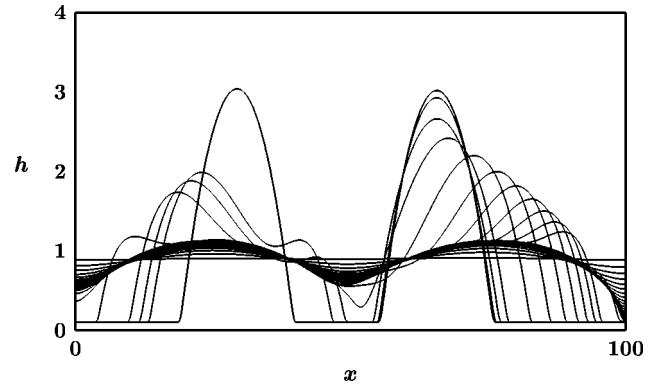


FIG. 4. A numerical simulation of the early stages of dewetting in thin films: instability of an initially uniform fluid layer (with  $h \approx 1$ ) leading to near-rupture of the film, the growth of holes in the layer (where  $h \sim \epsilon$ ), and the coalescence of the fluid into isolated droplets.

The parameter  $A$  is a universal constant given in terms of the molecular potential  $\mathcal{U}(\bar{H})$ , and determines the contact angle to leading order, independent of the ultrathin film scale  $\epsilon$  and the pressure  $\bar{p}$ . Moreover, the value of  $A$  gives an upper bound, independent of  $\epsilon$ , on the maximum slope of equilibrium solutions. This value also gives a leading order bound applicable to near-equilibrium solutions that we will consider later. The existence of such a uniform bound for the gradients of the solution  $h$  is necessary to maintain the applicability of the original lubrication approximation. Another important point is that Eq. (2.11) relates the interfacial energies to the contact angle, and is equivalent to the Young condition for shallow angles. This fact has been exploited by other authors for the purpose of numerical computations [35,36,48].

Finally, we define the droplet mass by that of the core region,

$$\bar{m}(\bar{p}) \equiv \int_{-w}^w \bar{h}(x; \bar{p}) dx \sim \frac{2A^3}{3\bar{p}^2}. \quad (2.12)$$

As a consequence, the size and mass of droplets may be measured in terms of the pressure  $\bar{p}$ . The error in this approximation of the mass is of the order of the thickness of the ultrathin film and vanishes as  $\epsilon \rightarrow 0$ . We will make use of Eq. (2.12) later to relate conservation of mass to an evolution equation for the droplet pressure.

### III. DYNAMICS OF THE ONE-DIMENSIONAL PROBLEM

Both analysis and numerical simulation identify a sequence of dynamical regimes for equation (1.11). Initially, a flat layer of fluid is subject to a long-wave instability (see Fig. 4). In the absence of conjoining effects in the pressure  $\Pi(h)$ , this instability would yield finite-time rupture of the fluid layer [39,40]. For potentials of the form of  $U(h)$ , the fluid dewets, it forms growing holes or dry spots [16] where the layer narrows down to an ultrathin film of height  $h \sim \epsilon$ . The fluid then rapidly converges to a series of parabolic-shaped droplets separated by the ultrathin film. Each droplet is very nearly an equilibrium solution like those already discussed. But there is a slow variation in the outer mean field (the ultrathin film) between neighboring droplets that leads

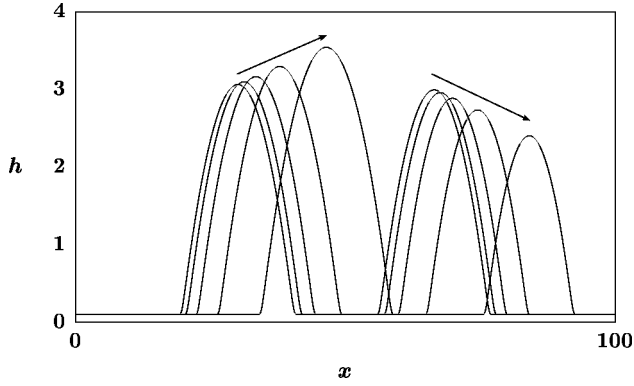


FIG. 5. Later stages in dewetting dynamics (continuing from Fig. 4): once formed, the near-equilibrium fluid droplets evolve on a slower time scale, with dynamics including both mass exchange and spatial drift.

to a coarsening process which governs the long-time evolution of the droplets.

Two features of the coarsening process are apparent (see Fig. 5). The first is that larger droplets gain mass at the expense of smaller droplets, in a fashion similar to Ostwald ripening. In our case, however, droplets also appear to move on time scales comparable to those of mass exchange. The causes for both of these phenomena will be explained next by a variational argument. A more systematic derivation of the dynamics follows.

#### Energy considerations

The slow process which ensues after the formation of metastable droplets may be understood by utilizing the mathematical structure of the evolution equation. Equation (1.11) has the energy

$$E(h) = \int U(h) + \frac{1}{2} h_x^2 dx, \quad (3.1)$$

which physically represents the sum of surface energy and intermolecular energies. In fact, Eq. (1.11) represents a generalized gradient flow (cf. [49]) of this energy and, subject to no-flux boundary conditions, the rate of energy dissipation is

$$\frac{dE}{dt} = - \int h^3 p_x^2 dx \leq 0. \quad (3.2)$$

There is an associated variational principle; the flux  $J = -h^3 p_x$  minimizes the functional

$$F(J) = - \int \delta E J_x dx + \frac{1}{2} \int \frac{J^2}{h^3} dx, \quad (3.3)$$

where the first variation of the energy (3.1) is  $\delta E = U'(h) - h_{xx} = p$ . Evaluated at the minimizer, the first term in this functional is just the change in energy

$$- \int \delta E J_x dx = \int \delta E h_t dx = \frac{dE}{dt}. \quad (3.4)$$

Similarly, the second term in Eq. (3.3) is minus one half times the rate of energy dissipation.

To demonstrate that the coarsening process is energetically favorable, we show that the merger of two equal-sized droplets to form a single larger droplet and an UTF layer yields a decrease in energy. Within each droplet core, the film satisfies  $h \gg \epsilon$ , therefore the potential energy is negligible, and hence, using Eq. (2.8)

$$E(\text{two droplets}) \sim 2 \int_{-\bar{w}}^{\bar{w}} \frac{1}{2} h_x^2 dx \sim \frac{2A^3}{3\bar{p}}, \quad (3.5)$$

where the half-width of each droplet is  $\bar{w} = A/\bar{p}$ , Eq. (2.8). For comparison, in a single droplet with mass  $2\bar{m}$ , the corresponding pressure is  $\bar{p} \sim \bar{p}/\sqrt{2}$  and the half-width is  $\bar{w} \sim \sqrt{2}A/\bar{p}$ . The merger of the two droplets creates an ultrathin layer with the length  $4\bar{w} - 2\bar{w} \sim (4 - 2\sqrt{2})A/\bar{p}$ . Hence the energy of the merged droplet is approximately

$$E(\text{single droplet and UTF}) \sim \frac{\sqrt{2}A^3}{3\bar{p}} + \frac{4 - 2\sqrt{2}}{\bar{p}} AU(\epsilon). \quad (3.6)$$

Not only is the surface energy of the droplet reduced relative to Eq. (3.5), but also the ultrathin film further reduces the energy since the potential  $U(\epsilon)$  is negative. Consequently, the total energy decreases as small droplets exchange mass through the UTF layer to form fewer, larger drops. This provides a driving force for the mass redistribution.

Since the energy is translation invariant, it may seem that there is no energetic advantage for droplets to move. Indeed, there is no energy lost in the translating process alone, and the first integral in Eq. (3.3) is essentially zero for a moving droplet. On the other hand, there may be nonzero fluxes imposed on the droplet by the ultrathin film on either side of the droplet. The flux minimizing the second term in Eq. (3.3) will therefore not be zero throughout the interior of the droplet, but rather is constrained to match the fluxes on either side of the droplet. As will be made precise in the following section, it is this flux which gives rise to droplet motion.

#### IV. DYNAMICS OF A SINGLE DROP

We now describe long-time metastable dynamics of dewetting films by first focusing on the dynamics of a single droplet. Following the complicated initial transient behavior in Eq. (1.11), the film will converge to form one or more near-equilibrium droplets, see Fig. 5. These droplets will interact and evolve on long time scales. The droplets will move and change mass in response to fluxes imposed on them through the ultrathin film mean field. To explain this behavior, we first consider the evolution of a single droplet on an interval,  $-L \leq x \leq L$ , that is large compared with the width of the droplet, with fluxes (1.13) imposed at the boundaries,

$$J(-L) = \sigma \tilde{J}_-, \quad J(L) = \sigma \tilde{J}_+, \quad (4.1)$$

where  $\sigma > 0$  is a small parameter, together with the boundary conditions,

$$h_{xxx}(-L) = 0, \quad h_{xxx}(L) = 0. \quad (4.2)$$

The latter conditions imposed on the ultrathin film correspond to the physical observation that away from the droplets, there is little variation in the curvature of the film; it will be shown that in the UTF the primary contribution to the flux is from the gradient of the disjoining pressure. These boundary conditions are needed to specify a well-posed problem for the fourth-order equation (1.11). Note that in the no-flux case,  $\bar{J}_- = \bar{J}_+ = 0$ , boundary conditions (4.1) and (4.2) reduce to  $h_x(\pm L) = h_{xxx}(\pm L) = 0$ , and yield the boundary value problem for equilibrium droplets on finite domains, considered in Ref. [24]. As an initial condition, we will use the equilibrium droplet solution, centered at  $x=0$ , with initial pressure  $\bar{p} = P_0$ , that is  $h_0(x) = \bar{h}(x; P_0)$ . For any finite domain,  $\bar{h}(x)$  is not an exact solution of the homogeneous boundary value problem, but it experiences only exponential small boundary influences and is called a quasiequilibrium solution by Ward [50]. We will neglect these small effects in the presence of finite fluxes.

Because droplets only change in response to the imposed fluxes, we introduce a new time scale selected by the scale of the fluxes,

$$\tau = \sigma t. \quad (4.3)$$

Later we will relate  $\sigma$  to the other parameters in the model. Assuming that the solution evolves quasistatically, we assume that the fluxes cause the position  $X(\tau)$  and pressure  $P(\tau)$  of the droplet to vary slowly in time and we seek a perturbation solution for  $\sigma \rightarrow 0$  of the form

$$h(x, t) = \bar{h}(x - X(\tau); P(\tau)) + \sigma h_1(x, \tau) + O(\sigma^2). \quad (4.4)$$

Substituting this ansatz into the evolution equation (1.11) to leading order in  $\sigma$  yields

$$-\frac{\partial \bar{h}}{\partial x} \frac{dX}{d\tau} + \frac{\partial \bar{h}}{\partial \bar{p}} \frac{dP}{d\tau} = \mathcal{L}h_1, \quad (4.5)$$

where  $\mathcal{L}$  is the linear operator for the spatial operator on the right side of Eq. (1.11),

$$\mathcal{L}g = \frac{\partial}{\partial x} \left( \bar{h}^3 \frac{\partial}{\partial x} \left[ \Pi'(\bar{h})g - \frac{\partial^2 g}{\partial x^2} \right] \right), \quad (4.6)$$

subject to the boundary conditions given by Eqs. (4.1), and (4.2). Since the leading term in Eq. (4.4) represents a two parameter  $(X, P)$  family of homogeneous equilibrium solutions of Eq. (1.11) and  $\mathcal{L}$  is a singular operator, the left side of Eq. (4.5) will need to satisfy two solvability conditions to ensure the existence of a unique solution for  $h_1$ . The solvability conditions, given by applications of the Fredholm alternative, are expressed in terms of orthogonality of the left side of Eq. (4.5) with the adjoint nullvectors, see Ward [50]. The operator  $\mathcal{L}$  is not self-adjoint; the adjoint operator is

$$\mathcal{L}^\dagger \psi = \left( \Pi'(\bar{h}) - \frac{\partial^2}{\partial x^2} \right) \left[ \frac{\partial}{\partial x} \left\{ \bar{h}^3 \frac{\partial \psi}{\partial x} \right\} \right]. \quad (4.7)$$

The null space of  $\mathcal{L}^\dagger$  is two dimensional and is spanned by the two bounded functions,

$$\psi_1(x) = 1, \quad \psi_2(x) = \int_0^x \frac{\bar{h}(x') - h_{\min}}{\bar{h}(x')^3} dx'. \quad (4.8)$$

Taking the inner product of  $\psi_1$  with Eq. (4.5) on  $[-L, L]$  gives an equation for the evolution of the droplet pressure,

$$\frac{dP}{d\tau} = \left( \int_{-L}^L \frac{\partial \bar{h}}{\partial \bar{p}} dx \right)^{-1} (\bar{J}_+ - \bar{J}_-), \quad (4.9)$$

where we have used the fact that  $\partial_x \bar{h}$  is an odd function with exponential decay outside of  $[-\bar{w}, \bar{w}]$  to eliminate the contribution of the first term on the left in Eq. (4.5). Similarly, taking the inner product of  $\psi_2$  with Eq. (4.5) using integration by parts, and again invoking even or odd symmetry gives an equation for the motion of the droplet,

$$\frac{dX}{d\tau} = - \left( \frac{\int_{-L}^L \frac{\bar{h} - h_{\min}}{\bar{h}^3} dx}{2 \int_{-L}^L \frac{(\bar{h} - h_{\min})^2}{\bar{h}^3} dx} \right) (\bar{J}_+ + \bar{J}_-). \quad (4.10)$$

At this point we note that  $\sigma$  is an artificial parameter, and we can eliminate it to write these two evolution equations in the original time scale and in terms of the unscaled fluxes as,

$$\frac{dP}{dt} = C_P(P, X)(J_+ - J_-), \quad \frac{dX}{dt} = -C_X(P, X)(J_+ + J_-), \quad (4.11)$$

where  $C_P$  and  $C_X$  are coefficient functions given by the integrals of the equilibrium droplet  $\bar{h}(x - X; P)$  in Eqs. (4.9), and (4.10).

We now examine the integrals in Eqs. (4.9) and (4.10) more closely to show that to leading order, these coefficients are only dependent on the droplet pressure  $P$ . In particular, we show that the dominant contributions to the coefficients are given by the droplet core and contact line regions, hence we reduce the integrals over the whole domain in Eqs. (4.9) and (4.10) to localized integrals over the droplet core. Consider  $C_X$ , since  $\bar{h}(x)$  approaches  $h_{\min}$  exponentially as  $|x| \rightarrow \infty$ , the integrands decay exponentially for  $|x| \gg \bar{w}$ , and we can either extend it to  $(-\infty, \infty)$  or truncate the range of integration to  $|x| \leq \bar{w}$  with only small errors, so that

$$C_X \sim C_X(P) = \left( \frac{\int_{-\bar{w}}^{\bar{w}} \frac{\bar{h} - h_{\min}}{\bar{h}^3} dx}{2 \int_{-\bar{w}}^{\bar{w}} \frac{(\bar{h} - h_{\min})^2}{\bar{h}^3} dx} \right). \quad (4.12)$$

In practice, we evaluate this coefficient using integrals over  $(-\infty, \infty)$  using the phase plane representation (2.3) of  $\bar{h}(x)$ , these integrals can be easily computed as singular integrals over  $h_{\min} \leq h \leq h_{\max}$ , the difference with exact evaluation of Eq. (4.12) is negligible. Note that since these integrals are translation invariant in  $x$ ,  $C_X$  is independent of  $X$ . From analysis of Eq. (4.12), it can be shown that  $C_X = O(\epsilon^{-1})$  as  $\epsilon \rightarrow 0$ .

A different approach must be applied to  $C_P$  since in the limit that  $L \rightarrow \infty$ , the integral in Eq. (4.10) diverges. This is because as  $|x| \rightarrow \infty$ ,  $\bar{h}(x) \rightarrow h_{\min}(\bar{p})$ , and as in Eq. (2.6),

$$\frac{dh_{\min}}{d\bar{p}} = O(\epsilon^2), \quad (4.13)$$

so that the contribution to the integral from the ultrathin film region will be  $O(L\epsilon^2)$ . As will be discussed further in the following section, we will restrict our attention to the regime where

$$\epsilon^2 L \ll 1. \quad (4.14)$$

Then the contribution from the ultrathin film region will be negligible, and we can approximate the integral with one over only the droplet core

$$C_P \sim C_P(P) = \left( \int_{-\bar{w}}^{\bar{w}} \frac{\partial \bar{h}}{\partial \bar{p}} dx \right)^{-1}, \quad (4.15)$$

to within  $O(\epsilon^2)$  errors. We calculate this coefficient from the definition of droplet mass (2.12), so that

$$C_P(P) = \left( \frac{d}{d\bar{p}} \bar{m}(\bar{p}) \right)^{-1} \sim -\frac{4\bar{p}^3}{3A^3}. \quad (4.16)$$

From Eq. (4.16), also notice that equation (4.9) is just a statement of conservation of mass in the form

$$\frac{dm}{dP} \frac{dP}{dt} = J_+ - J_-. \quad (4.17)$$

Notice that moving contact lines occur in this model as a result of droplet drift or changes in mass. Accompanying the motion of the contact lines there will also be modifications to the equilibrium droplet shape, given to leading order by the solution of Eq. (4.5) for  $h_1(x, \tau)$ . Many authors have pointed out serious fundamental problems regarding the motion of contact lines in lubrication models that neglect the influence of the disjoining pressure [30,36,51,52]. The inclusion of the effect of intermolecular forces in the mathematical model (1.11) overcomes these problems [36]. As we will show in the following section, for the long-time dynamics of dewetting films, the relevant scale for the fluxes imposed on the droplets is small,  $J = O(\epsilon^3/L)$ . Therefore, in the absence of other external forces, the droplets will remain very close to equilibrium, with  $O(\epsilon^3)$  corrections to  $\bar{h}(x - X(t); P(t))$  in Eq. (4.4). The near-equilibrium model of droplet dynamics given by Eq. (4.11) can be expected to hold while the evo-

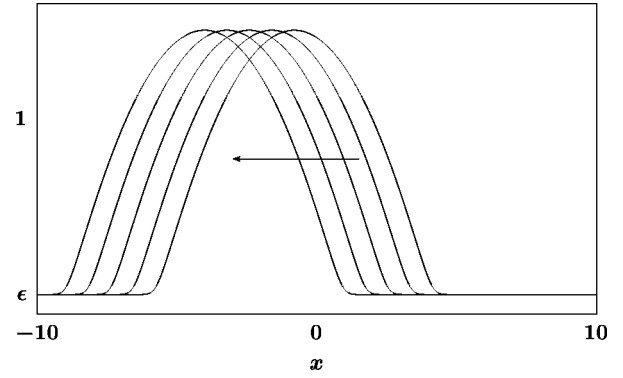


FIG. 6. The slow translational motion of a near-equilibrium droplet solution of Eq. (1.11) due to equal imposed fluxes,  $\bar{J}_+ = \bar{J}_-$ , Eq. (4.10).

lution of the droplets is slow, with the velocity being  $O(\epsilon^2/L)$  or smaller and  $O(\epsilon^3)$ -corrections to the static contact angle  $\theta = \tan^{-1}A$  for advancing and receding contact lines.

We conclude this section by illustrating the two special cases for the evolution laws (4.11) in which the two equations decouple.

(1) If  $J_+ = J_-$ , then  $dP/dt = 0$ , hence there is no change in pressure or mass of the droplet; this yields a pure translational mode, see Fig. 6. In fact, since  $C_X(P)$  is fixed, if the fluxes are held constant, then the solution is a constant velocity traveling pulse,  $h \sim \bar{h}(x - ct; P)$ .

(2) If  $J_+ = -J_-$ , then  $dX/dt = 0$ , hence there is no change in the position of the droplet; this is a pure change-of-mass (pressure) mode, see Fig. 7. For large drops (with small  $\bar{p}$ ), the scaling relations found earlier suggest that this mode of evolution can be approximately described by a self-similar solution of the form  $h(x, t) \sim \mathcal{H}(x/P(t))/P(t)$ . In the following section we go on to study how the dynamics of a single droplet given by Eq. (4.11) can be used to describe the coupled dynamics of an array of interacting droplets.

## V. DYNAMICS OF ARRAYS OF INTERACTING DROPLETS

We now make use of Eq. (4.11) as a building block to describe the dynamics for problems with multiple drops [53],

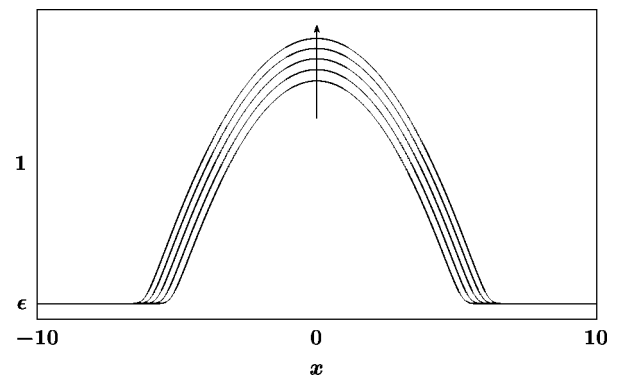


FIG. 7. The slow mass growth of a near-equilibrium droplet solution of Eq. (1.11) due to opposite imposed fluxes,  $\bar{J}_+ = -\bar{J}_-$ , Eq. (4.9).

the generic case of interest for dewetting films, where large numbers of droplets are typically initially formed.

Suppose that several droplets are present, connected to each other by an ultrathin fluid layer with  $h \sim \epsilon$ . In this case, the fluxes imposed on each droplet are due to neighboring drops. Our goal is to derive asymptotically valid expressions for the fluxes  $J_{\pm}$  (1.13) which then may be used to completely describe the evolution of droplets by using Eq. (4.11). This will involve a more careful examination of the structure of the ultrathin film between the droplets.

Let  $L$  be a typical distance between droplets, which is assumed large but not so large as to violate Eq. (4.14). In the UTF, rescale space using the new coordinate  $z = \delta x$  where  $\delta = L^{-1}$  is a small quantity. We also scale the film thickness by  $h = \epsilon H$ . For droplets with fixed mass (and hence fixed pressure), the fluxes between drops will have the scale  $O(\epsilon^3 \delta)$ , so the time scale (4.3) is set by

$$\tau = \epsilon^3 \delta t. \quad (5.1)$$

In terms of the rescaled variables and Eq. (1.8), Eq. (1.11) yields the equation for the ultrathin film outside the droplet cores,

$$\epsilon^2 \delta^{-1} \frac{\partial H}{\partial \tau} = \frac{\partial}{\partial z} \left( H^3 \frac{\partial}{\partial z} \left[ \mathcal{U}'(H) - \epsilon^2 \delta^2 \frac{\partial^2 H}{\partial z^2} \right] \right). \quad (5.2)$$

First we note that for  $\epsilon, \delta \rightarrow 0$ , the last term in Eq. (5.2) is always negligible; this corresponds to the physical expectation that the curvature of the UTF is negligible compared to its disjoining pressure. Hence, to leading order Eq. (5.2) becomes the second-order nonlinear diffusion equation,

$$\epsilon^2 \delta^{-1} \frac{\partial H}{\partial \tau} = \frac{\partial^2}{\partial z^2} [\mathcal{V}(H)], \quad (5.3)$$

where the ‘‘chemical potential’’ function  $\mathcal{V}(H)$  is defined (up to an additive constant) by

$$\frac{d\mathcal{V}}{dH} = H^3 \frac{d^2 U}{dH^2}. \quad (5.4)$$

In terms of the unscaled variables, we may define the corresponding quantity

$$\frac{dV}{dh} = h^3 \frac{d^2 U}{dh^2} \quad (5.5)$$

so that  $V(h)$  is just a rescaling of  $\mathcal{V}(H)$ ,

$$V(h) = \epsilon^2 \mathcal{V}(h/\epsilon). \quad (5.6)$$

Notice that the (unscaled) flux between droplets is therefore

$$J = -\partial_x V(h). \quad (5.7)$$

From Eq. (5.3) we note that if our assumption (4.14) on the thickness of the UTF compared to the separation length between droplets holds, then the ultrathin film evolves quasistatically, slaved to the evolution of the droplets. The struc-

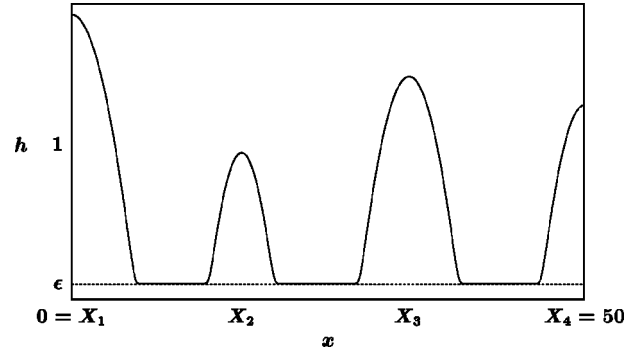


FIG. 8. The film thickness at time  $t=8000$  (after initial transients have vanished) from a numerical solution of Eq. (1.11) for  $\epsilon=0.1$  showing four well-defined drops with a connective ultrathin film.

ture of the ultrathin film is then given by a solution of  $\partial_{xx} V(h) = 0$  subject to the boundary conditions that  $V(h)$  at a contact line is  $V(h_{\min})$  for that particular drop. Consequently, we obtain that the flux  $-dV/dx$  between droplets is constant. In particular, the flux between two neighboring drops, labeled by  $k$  and  $k+1$  and characterized by their positions  $X$  and pressures  $P$ , is given by

$$J_{k,k+1} = -\frac{V(h_{\min}(P_{k+1})) - V(h_{\min}(P_k))}{[X_{k+1} - \bar{w}(P_{k+1})] - [X_k + \bar{w}(P_k)]}. \quad (5.8)$$

Since the thickness of the ultrathin film varies by only a small amount, the mobility coefficient in the definition of the flux (1.13) is always of the order  $h^3 \sim \epsilon^3$ . We conclude that since the flux is approximately constant, the pressure in the UTF is approximately piecewise linear. This is born out by the results of numerical simulations of Eq. (1.11), see Figs. 8, 9.

In summary, we have reduced Eq. (1.11) to a system of  $2N$  ordinary differential equations for the evolution of positions  $X_k$  and pressures  $P_k$  of an array of  $N$  drops,

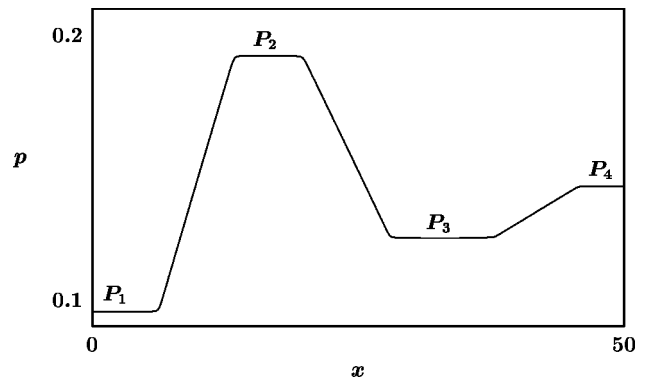


FIG. 9. The corresponding pressure (1.12) at  $t=8000$  for the solution shown in Fig. 8. Note the near-constant pressure plateaus corresponding to the cores of the near-equilibrium droplets.

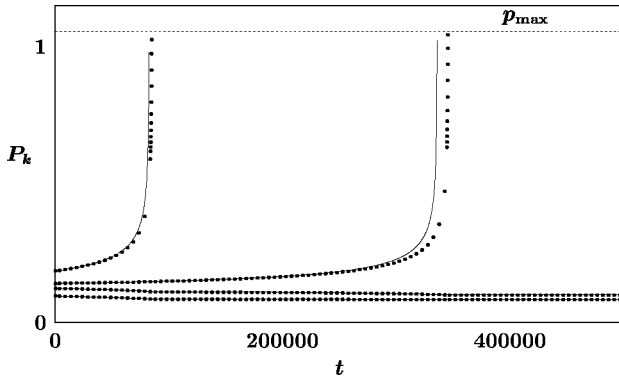


FIG. 10. Comparison of predictions for droplet pressures  $P_k(t)$  from the direct numerical solution of the PDE (1.11) (dots) and the ODE model of coarsening (5.9) (solid curves) for the problem shown in Fig. 8. Note the collapse of two droplets as  $P_2$  and  $P_4$  exceed  $p_{\max}$  in finite time.

$$\frac{dP_k}{dt} = C_P(P_k)(J_{k+1,k} - J_{k,k-1}), \quad (5.9)$$

$$\frac{dX_k}{dt} = -C_X(P_k)(J_{k+1,k} + J_{k,k-1}), \quad k=1,2,\dots,N,$$

where the fluxes are defined by Eq. (5.8) and the coefficient functions are given by Eqs. (4.12) and (4.15).

These equations were integrated numerically using a fourth-order Runge-Kutta scheme with an adaptive time step. If a droplet shrinks in size, its mass decreases and hence by Eq. (2.12) its pressure increases. The pressure of the droplet will eventually become larger than  $p_{\max}$ , at which point the droplet is no longer near an equilibrium state. These “collapsing” droplets are very small and rapidly become part of the UTF mean field, so they are simply deleted from the array of finite drops when this occurs. Comparison of this coarsening model to the dynamics of the PDE for a small array of drops is shown in Figs. 10, 11.

The second equation in Eq. (5.9) allows for motion of the droplets and hence the possibility of collisions between them. For practical computation of Eq. (5.9), we identify the

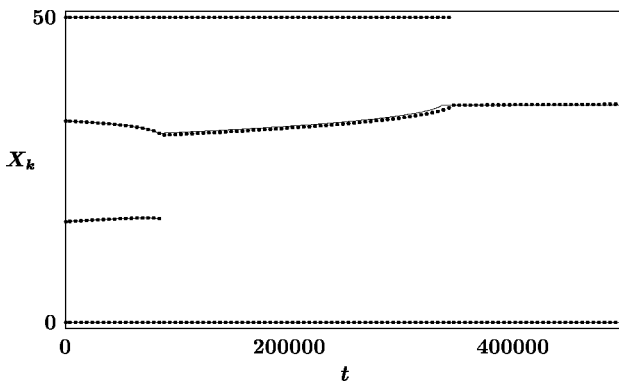


FIG. 11. Comparison of predictions for droplet positions  $X_k(t)$  from the direct numerical solution of the PDE (1.11) (dots) and the ODE model of coarsening (5.9) (solid curves) for the problem shown in Fig. 8. The termination of the  $X_2$  and  $X_4$  branches occurs when those droplets collapse.

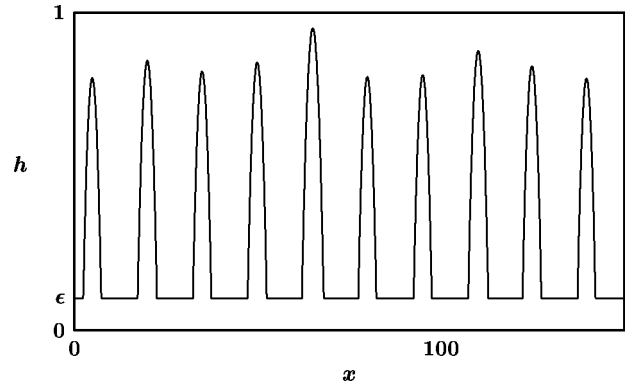


FIG. 12. Profiles of a typical subset of widely spaced, nearly identical droplets considered in the analysis of the scaling properties of the coarsening process.

onset of a collision when the contact lines of two neighboring droplets are within a  $O(\epsilon)$  distance from each other. The dynamics of collisions are far from equilibrium, and hence occur on short time scales compared to the near-equilibrium coarsening process. Neglecting the time of collision, the two drops are replaced by a single larger droplet with a pressure corresponding to the total mass of the two drops. The position of the resulting droplet was determined by the center of mass of the colliding droplets.

## VI. SCALING LAW FOR THE DROPLET COARSENING PROCESS

Dewetting instabilities of nearly uniform layers in large systems can be expected to form large numbers of droplets with comparable masses and similar separation distances [17,18]. For long times, the arrays of droplets will evolve slowly according to the coarsening dynamics derived above. For such problems, the computational costs of direct simulations of the PDE (1.11) are prohibitive. Noting the time scales in Figs. 10 and 11, the solution of Eq. (5.9) for large arrays for very long times can also become very costly. As an alternative to these numerical approaches, and to gain more insight into the physical mechanisms of the coarsening process in this problem, we derive a power-rule scaling law for the average number of drops at, as a function of time,  $N(t)$ . We now consider the coarsening dynamics for large arrays of drops,  $N \rightarrow \infty$ . As an example, we solve Eq. (5.9) starting from  $N=1000$  droplets of nearly equal mass, with large but nearly uniform spacing between adjacent droplets,  $L$ , see Fig. 12. Figure 13 shows the  $X_k(t)$  world lines for the positions of a typical subset of droplets in the array. In this example, there is relatively little drift of the droplets compared to their average spacing, so there were no collisions; the termination of  $X_k(t)$  lines indicates the collapse of those droplets. A log-log plot of the number of drops as a function of time for this simulation shows good agreement with a scaling law of the form

$$N(t) = O(t^{-2/5}), \quad (6.1)$$

see Fig. 14. This behavior is reproduced for the long-time behavior from broad classes of initial data and appears to be

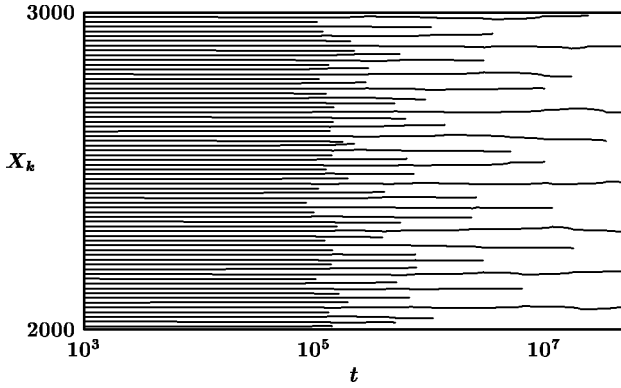


FIG. 13. World lines  $X_k(t)$  for a set of drops in a large array from a simulation of the coarsening dynamics given by Eq. (5.9).  $X_k(t)$  lines end when a droplet collapses to negligible mass.

the generic behavior of the coarsening process. We now present a heuristic argument for the occurrence of this power-law scaling behavior in the coarsening dynamics for dewetting.

This scaling behavior can be derived by considering the dynamics given by Eq. (5.9) that control the collapse of a single typical droplet in the array. Let this drop, with index  $k$ , have somewhat smaller mass (and hence higher pressure  $P_k$ ) than its neighbors. We will assume that the separation between droplets,  $L$  is relatively large, so that we can neglect the droplet motion and focus on the equation for the evolution of the droplet pressures. By Eq. (4.16), we have  $C_P \propto P^3$ , and from Eq. (5.9) it is clear that droplets with larger pressures (that is smaller masses) evolve on faster time scales. In fact, we will show that the collapse of small droplets occurs in finite time. Using Eq. (2.6), to leading order the chemical potential yields  $V(h_{\min}) \sim \epsilon^3 P$ . Consequently, the flux (5.8) is approximated to leading order by

$$J_{k,k+1} \sim -\frac{\epsilon^3 P_{k+1} - \epsilon^3 P_k}{L}. \quad (6.2)$$

Here we have assumed that  $L \approx X_{k+1} - X_k$  is large compared to the average droplet width and that we can neglect the

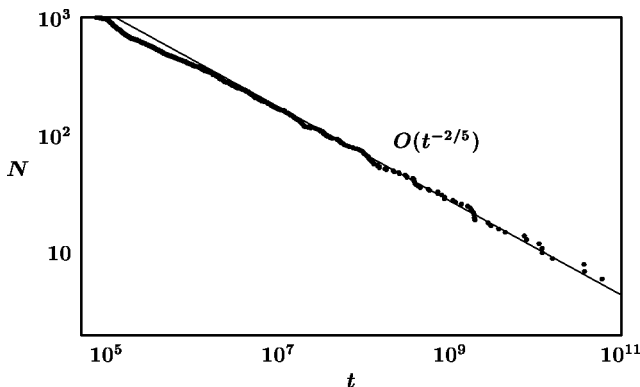


FIG. 14. Log-log plot of the number of drops as a function of time. A line corresponding to the scaling law (6.1) is shown for comparison.

influence of droplet motion on the time scale for pressure evolution. Therefore, the pressure evolution equation becomes

$$\frac{dP_k}{dt} \propto \frac{\epsilon^3}{L} P_k^3 (P_{k+1} - 2P_k + P_{k-1}). \quad (6.3)$$

Since we have assumed that  $P_k \gg P_{k\pm 1}$ , the time scale for the evolution of  $P_k$  is much faster than that of its neighbors, therefore this equation further reduces to the local model,

$$\frac{dP_k}{dt} \propto -\frac{1}{L} P_k^4. \quad (6.4)$$

The solution of this model shows collapse of the droplet in a finite time, as the pressure diverges as  $t \rightarrow T_c$ ,

$$P_k(t) \propto \left( \frac{T_c - t}{L} \right)^{-1/3}. \quad (6.5)$$

If the initial pressure of the collapsing drop is  $\bar{P}_k$ , then its collapse time scales like

$$T_c \propto \bar{P}_k^{-3} L. \quad (6.6)$$

The typical droplet pressure relates to the mass by  $M \propto \bar{P}^{-2}$  [see Eq. (2.12)]. Both  $M$  and  $L$  scale like  $N^{-1}$  by the conservation of mass and the definition of the average separation distance on a finite size system, respectively. Therefore Eq. (6.6) yields the relation for the collapse time scale of the  $N$ th droplet,

$$T_c \propto N^{-5/2}. \quad (6.7)$$

Note that during the collapse of each droplet, we assume that the separation distance  $L$  is approximately fixed. Although individual droplets will move, it seems evident again from the numerical simulations that the *average* droplet spacing will be unaffected. Therefore, the scaling (6.7) should be correct when averaged over a large number of droplets. We also assume that  $L$  varies on a slower time scale in response to reduction in the number of droplets due to collapse of individual drops, consistent with our assumption that the motion of droplets is slower than the evolution of pressures.

As can be seen from Fig. 13, as time progresses, a roughly constant fraction of droplets vanish per unit time. We assume that the droplet collapses are independent uncorrelated events. Therefore, at a given time a constant fraction of droplets will be collapsing, which means that the droplet number  $N(t)$  satisfies

$$\frac{dN}{dt} \propto -\frac{N}{T_c} \propto -N^{7/2}. \quad (6.8)$$

This may be integrated to yield the desired scaling relation,

$$N \propto t^{-2/5}. \quad (6.9)$$

## VII. DISCUSSION AND CONCLUSIONS

We have given an asymptotic description of the late-stage coarsening dynamics of a one-dimensional dewetting thin film. A similar description is anticipated for two-dimensional films, where the interdroplet flux will be derived from a two-dimensional elliptic boundary value problem analogous to Eq. (5.3). We also expect that a scaling law for the droplet number can be derived for two-dimensional films, which would be highly useful for comparison with experiments.

A further challenge is to understand the asymptotics for small  $\epsilon$  of droplets far from equilibrium. Since the addition of conjoining forces provides a regularization of problems for the motion of contact lines, the limiting dynamics for small  $\epsilon$  may provide insight into the connections between intermolecular forces and macroscopic models for contact

line motion.

Our work has implications for coarsening processes in general. In certain regimes, it seems possible that collision of droplets, as opposed to their collapse, is the mechanism responsible for coarsening. Because the mathematical structure of our model is similar to those describing coarsening of binary mixtures, interface motion may be important for these processes as well.

## ACKNOWLEDGMENTS

We thank Andy Bernoff, Andrea Bertozzi, and John Neu for useful suggestions. This research was supported by NSF FRG Grant No. DMS-0074049. T.P.W. was also financially supported by the Alfred P. Sloan Foundation.

- 
- [1] R. Konnur, K. Kargupta, and A. Sharma, *Phys. Rev. Lett.* **84**, 931 (2000).
- [2] G. Reiter, *Phys. Rev. Lett.* **68**, 75 (1992).
- [3] G. Reiter, A. Sharma, A. Casoli, M.-O. David, R. Khanna, and P. Auroy, *Langmuir* **15**, 2551 (1999).
- [4] A. Sharma and R. Khanna, *Phys. Rev. Lett.* **81**, 3463 (1998).
- [5] A. Sharma and R. Khanna, *J. Chem. Phys.* **11**, 4929 (1999).
- [6] R. Xie, A. Karim, J.F. Douglas, C.C. Han, and R.A. Weiss, *Phys. Rev. Lett.* **81**, 1251 (1998).
- [7] S. Herminghaus, K. Jacobs, K. Mecke, J. Bischof, A. Fery, M. Ibn-Elhaj, and S. Schlagowski, *Science* **282**, 916 (1998).
- [8] M.P. Valignat, S. Villette, J. Li, R. Barberi, R. Bartolino, E. Dubois-Violette, and A.M. Cazabat, *Phys. Rev. Lett.* **77**, 1994 (1996).
- [9] F. Vandenbrouck, M.P. Valignat, and A.M. Cazabat, *Phys. Rev. Lett.* **82**, 2693 (1999).
- [10] J. Bischof, D. Scherer, S. Herminghaus, and P. Leiderer, *Phys. Rev. Lett.* **77**, 1536 (1996).
- [11] M. Elbaum, S.G. Lipsom, and J.F. Wettlaufer, *Europhys. Lett.* **29**, 457 (1995).
- [12] A. Oron and S.G. Bankoff, *J. Colloid Interface Sci.* **218**, 152 (1999).
- [13] J.W. Cahn and J.E. Hilliard, *J. Chem. Phys.* **28**, 258 (1957).
- [14] V.S. Mitlin, *J. Colloid Interface Sci.* **156**, 491 (1993).
- [15] V.S. Mitlin and N.V. Petviashvili, *Phys. Lett. A* **192**, 323 (1994).
- [16] A. Ghatak, R. Khanna, and A. Sharma, *J. Colloid Interface Sci.* **212**, 483 (1999).
- [17] U. Thiele, M.G. Velarde, K. Neuffer, and Y. Pomeau, *Phys. Rev. E* **64**, 031602 (2001).
- [18] U. Thiele, M.G. Velarde, and K. Neuffer, *Phys. Rev. Lett.* **87**, 016104 (2001).
- [19] B.D. Yang and O.C.K. Tsui, e-print cond-mat/0110123(1).
- [20] J. Becker, G. Grun, R. Seemann, and K. Jacobs, Dynamical pattern formation upon dewetting. LANL e-print cond-mat/0106313(1).
- [21] R. Seemann, S. Herminghaus, and K. Jacobs, *Phys. Rev. Lett.* **86**, 5534 (2001).
- [22] R. Seemann, S. Herminghaus, and K. Jacobs, *Phys. Rev. Lett.* **87**, 196101 (2001).
- [23] R.A. Segalman and P.F. Green, *Macromolecules* **32**, 801 (1999).
- [24] A.L. Bertozzi, G. Grun, and T.P. Witelski, *Nonlinearity* **14**, 1569 (2001).
- [25] J.N. Israelachvili, *Intermolecular and Surface Forces*, 2nd ed. (Academic Press, New York, 1992).
- [26] H. Ockendon and J.R. Ockendon, *Viscous Flow* (Cambridge University Press, Cambridge, 1995).
- [27] A. Oron, S.H. Davis, and S.G. Bankoff, *Rev. Mod. Phys.* **69**, 931 (1997).
- [28] C. Bauer and S. Dietrich, *Phys. Rev. E* **60**, 6919 (1999).
- [29] S. Dietrich and M. Napiorkowski, *Phys. Rev. A* **43**, 1861 (1991).
- [30] P.G. de Gennes, *Rev. Mod. Phys.* **57**, 827 (1985).
- [31] A. Oron and S.G. Bankoff, *Phys. Fluids* **13**, 1107 (2001).
- [32] J. Lopez, C.A. Miller, and E. Ruckenstein, *J. Colloid Interface Sci.* **56**, 460 (1976).
- [33] M.B. Williams and S.H. Davis, *J. Colloid Interface Sci.* **90**, 220 (1982).
- [34] J.P. Burelbach, S.G. Bankoff, and S.H. Davis, *J. Fluid Mech.* **195**, 463 (1988).
- [35] L.W. Schwartz, R.V. Roy, R.R. Eley, and S. Petrash, *J. Colloid Interface Sci.* **234**, 363 (2001).
- [36] L.W. Schwartz, in *Free Surface Flows With Viscosity* (Computational Mechanics Publications, Boston, 1997), pp. 203–233.
- [37] L. Pismen and Y. Pomeau, *Phys. Rev. E* **62**, 2840 (2000).
- [38] L. Pismen, *Phys. Rev. E* **64**, 021603 (2001).
- [39] T.P. Witelski and A.J. Bernoff, *Phys. Fluids* **11**, 2443 (1999).
- [40] W.W. Zhang and J.R. Lister, *Phys. Fluids* **11**, 2454 (1999).
- [41] G. Grün and M. Rumpf, *Numer. Math.* **87**, 113 (2000).
- [42] J.W. Cahn, C.M. Elliott, and A. Novick-Cohen, *Eur. J. Appl. Math.* **7**, 287 (1996).
- [43] R.L. Pego, *Proc. R. Soc. London, Ser. A* **422**, 261 (1989).
- [44] I.M. Lifshitz and V.V. Slyozov, *J. Chem. Phys. Solids* **19**, 35 (1961).
- [45] C. Wagner, *Z. Elektrochem.* **65**, 581 (1961).
- [46] V. Mitlin, *J. Colloid Interface Sci.* **227**, 371 (2000).
- [47] V. Mitlin, *J. Colloid Interface Sci.* **233**, 153 (2001).
- [48] H.S. Wong, S. Morris, and C.J. Radke, *J. Colloid Interface Sci.* **148**, 317 (1992).

- [49] F. Otto, Arch. Ration. Mech. Anal. **141**, 63 (1998).
- [50] M.J. Ward, in *Multiple-time-scale Dynamical Systems* (Springer, New York, 2001), pp. 233–259.
- [51] E.B. Dussan, V. Davis, and S.H. Davis, J. Fluid Mech. **65**, 71 (1974).
- [52] C. Huh and L.E. Scriven, J. Colloid Interface Sci. **35**, 85 (1971).
- [53] C. Elphick, E. Meron, and E.A. Spiegel, SIAM (Soc. Ind. Appl. Math.) J. Appl. Math. **50**, 490 (1990).